JCTC Journal of Chemical Theory and Computation

Computational Study of Promising Organic Dyes for High-Performance Sensitized Solar Cells

David Casanova,*,† François P. Rotzinger,‡ and Michael Grätzel‡

Institut de Química Teòrica i Computacional (IQTCUB), Universitat de Barcelona, Martí i Franquès, 1-11, 08028 Barcelona, Spain, and Institut des Sciences et Ingénierie Chimiques (ISIC), Laboratoire de Photonique et Interfaces, Ecole Polytechnique Fédérale de Lausanne (EPFL), CH-1015 Lausanne, Switzerland

Received October 27, 2009

Abstract: The energy transition from the ground state to the first excited singlet of four organic dye candidates to be used as sensitizers in solar cells, D5, D7, D9, and D11, has been computationally explored and compared to experimental results with TDDFT (B3LYP, ωB97, and ωB97X functionals) and the CIS(D) and SOS-CIS(D) wave function based methods. The second-order perturbation correction to CI singles' excitation energies are superior to any TDDFT functional employed here. The performance of SOS-CIS(D) is especially interesting, being in good agreement with absorption spectra and having important computational savings. The best TDDFT results are obtained by the ωB97X functional. Solvation effects on the excitation energies have been studied with three different models, i.e., the Onsager reaction field model, SS(V)PE, and SM8.

Introduction

Dye-sensitized solar cells are alternatives to conventional semiconductor photovoltaic devices. With ruthenium polypyridyl dyes, up to 11% conversion efficiency at standard AM 1.5 sunlight has been achieved.[1,2] Metal-free organic dyes are promising alternatives because of their high extinction coefficients. With such compounds, efficiencies of ∼4−8% have been reached so far.[3–6] To improve their yield, the light-absorption maximum needs to be shifted to the red, and the interaction of the excited (injecting) state of the dye with the conduction band of the semiconductor, on whose surface the dye is anchored, has to be improved.

One of the most recent studies in this direction corresponds to the analysis of four organic dye-sensitizers, e.g., 3-(5-(4-(diphenylamino)styryl)thiophen-2-yl)-2-cyanoacrylic acid (D5),[6] 3-(5-bis(4-(diphenylamino)styryl)thiophen-2-yl)-2-cyanoacrylic acid (D7), 5-(4-(bis(4-methoxyphenylamino)-styryl)thiophen-2-yl)-2-cyanoacrylic acid (D9), and 3-(5-bis(4,4′ -dimethoxydiphenylamino)styryl)thiophen-2-yl)-2-cyanoacrylic acid (D11). These molecules (Figure 1) were synthesized, anchored onto TiO_2, and tested in dye-sensitized solar cells, showing promising photon-to-current conversion efficiencies.[7]

From the experimental point of view, the syntheses of such sensitizers are quite demanding. Therefore, one would like to predict beforehand the potential properties of possible candidates in order to screen out molecules without the desired qualities and find those systems worth testing experimentally. To do that in a comprehensive and systematic manner, one could try to find some answers using the available quantum chemistry methods. Computational studies can be really helpful in providing some hints about the important aspects of the studied molecules, like the prediction of transition energies, oscillator strengths, or the electronic nature of the ground and excited states. But, first of all, these methods must be validated in the computation of the target molecules, and the comparison to experimental measurements is mandatory. These results should provide a standardized procedure to be applied in the study of similar sets of organic dyes.

In the computation of electronic excited states, a large variety of molecular quantum chemistry methods is available. The hierarchy of the approximations defines the properties of the models, classifying them at different levels of

* Corresponding author e-mail: davidcasanovacasas@ub.edu.
† Universitat de Barcelona.
‡ EPFL.

10.1021/ct100069q
Published on Web 03/15/2010

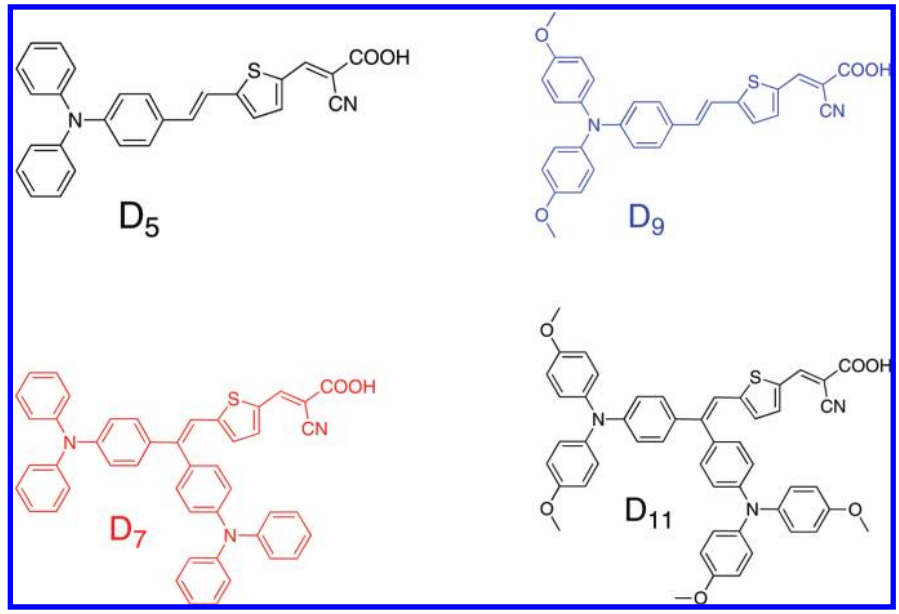

Figure 1. Molecular structures of D5, D7, D9, and D11 dye sensitizers.

complexity. Of course, the chosen computation level will directly affect on the accuracy of the computed energy, but it also determines its computational cost. Although quite high accuracy is desired in the calculation of transition energies of organic dyes (ideally, one would like to achieve an accuracy better than ~0.05 eV), computational demands are rather worrisome, especially due to the size of the molecules with the targeted properties. Thus, accurate models in the determination of single electron character excitation energies like the equation-of-motion coupled cluster (EOM-CC)[8–12] family of methods, the closely related linear response coupled-cluster (LR-CC),[13,14] or the symmetry-adapted cluster configuration interaction (SAC-CI)[15–17] methods cannot be considered in routine screenings of transition energies of such large molecules. These limitations become even stronger in multiconfigurational-based wave function methods, like multireference configuration interaction (MR-CI),[18] mutlireference coupled-cluster (MRCC),[19,20] or second-order perturbation correction to the complete active space self-consistent field (CASPT2[21] or MCQDPT2,[22,23] for example), which seem, in general, computationally prohibitive. Methods allowing for larger active spaces for the multiconfiguration SCF wave function (MCSCF) reference are available, in particular, second-order perturbation theory (PT2) based on restricted active space SCF (RASPT2)[24] or PT2 based on general MCSCF (GMCPT2).[25–27]

On the other hand, although time-dependent density functional theory (TDDFT)[28,29] represents a very attractive alternative, the standard density functionals exhibit a sizable delocalization and static correlation error,[30] as well as the self-interaction[31] error. The latter is responsible for large errors in long-range charge transfer transition energies[32–36] and becomes rather relevant in the kind of excitations occurring in molecular dyes. Therefore, one has to be very careful in drawing some conclusions derived from the application of such a methodology.

The present article reports on the computation of the lowest-energy electronic singlet-to-singlet transitions of metal-free organic dyes (Figure 1) used in dye-sensitized solar cells. These electronic excitations have been explored within the configuration interaction singles (CIS),[15] its second-order perturbation correction CIS(D)[37,38] and the scaled opposite spin version SOS-CIS(D),[39] and by TDDFT[28,29] using the popular B3LYP[40,41] functional and the recently developed long-range corrected (LC) ωB97 and ωB97X hybrid density functionals of Chai and Head-Gordon,[42] which substantially reduce standard long-range errors. The computed values are compared to experimental spectra. The available experimental UV−vis spectra were measured in ethanol solution. Since the charge transfer absorption bands can be very sensitive to the solvent polarity and hydrogen bonding, the effect of the solvent on excitation energies of D5, D7, D9, and D11 sensitizers was also taken into account.

The exposition of the present study is as follows. First, a detailed description of the computational tools employed is introduced. Second, a discussion of the obtained results based on the comparison to the available experimental data is presented. Finally, the main conclusions are exposed.

Computational Details

Geometry optimizations of the D5, D7, D9, and D11 organic sensitizers (Figure 1) in the ground state and in ethanol solution have been performed with no symmetry restrictions at four different computational levels: B3LYP, ωB97, and ωB97X and at the scaled opposite spin MP2 (SOSMP2).[43,44] All geometry optimizations were computed in ethanol solution using the SM8 solvation model,[45] and with the 6-31G(d) basis set.[46,47] The discussed results correspond to B3LYP/6-31G(d) geometries unless indicated. The vertical excitation energies were calculated for all geometries by CIS,[15] CIS(D),[37,38] and SOS-CIS(D)[39] wave-function-based methods, and by the B3LYP, ωB97, and ωB97X functionals[42] within the TDDFT methodology. The 6-31+G(d) basis set has been used for all of the cases. The resolution-of-the-identity (RI) approximation[48,49] and the adoption of the

Laplace transform[50] in the integral evaluations were used in the CIS(D) and SOS-CIS(D) calculations. TDDFT energies were obtained within the Tamm−Dancoff (TDA) approximation.[51] All transitions were computed at the gas phase and ethanol solution. Three different solvation models were compared in the computation of transition energies: the Onsager reaction field model[52] up to the 15th multipole order expansion, Surface and Simulation of Volume Polarization for Electrostatics (SS(V)PE),[53–55] and the SM8 solvation model. In the Onsager and SS(V)PE cases, the solute−solvent interaction was described through the definition of a spherical cavity for the solute molecule. The radius of the cavities was defined as half the distance between the two outermost atoms of the solute molecule plus 1.4 Å to ensure that it was fully contained in the cavity. In the SM8 model, the solute cavities are defined by the superposition of nuclear-centered spheres whose sizes are determined by intrinsic atomic Coulomb radii. The employed value of the static dielectric constant for ethanol solvent was 24.85. Vertical excitation energies in solution have been computed within the equilibrium solvation approach. The 6-31G(d) basis was used in the comparison of the solvation models. Vibronic couplings have been neglected throughout the present study. All calculations were performed with the Q-Chem program.[56]

Results and Discussion

The chemical structure of the studied dyes, i.e., D5, D7, D9, and D11, is composed of three modules: a triarylamine group acting as an electron donor, a thiophene which can be seen as an electron conductor, and an acceptor carrying the anchoring group, the cyano-acrylate fragment. This composition determines the general electronic properties of the D*n* molecules, and it further draws the boundaries of their spectroscopic behavior. In the D5 dye optimized geometry, the fragment constituted by the cyano-acrylate, the thiophene, and the chemically bonded benzene ring of the triarylamine group presents a planar space disposition, while the two benzene rings at one end of the molecule lie out of the plane (with dihedral angles to the plane between 60° and 90°). Besides the methoxy substitution in D9, there are almost no geometrical differences between D5 and D9 molecules, and only the dihedral angle between the two out of plane benzene rings of the triarylamine slightly increases from D5 to D9 (∼78° and ∼86°, respectively). The introduction of a second triarylamine group in D7 with respect to the D5 dye implies some relatively important structural modifications. The planarity observed in D5 and D9 cases is no longer preserved; i.e., any of the benzene rings appear coplanar to the thiophene and cyano-acrylate fragments. It is also worth mentioning the fact that, while one of the triarylamine groups has a rather linear disposition with respect to the thiophene and cyano-acrylate fragments, the second one appears in a quite perpendicular orientation with respect to the main molecular direction. As in the D5/D9 case, there are no relevant geometrical differences between D7 and D11 optimized geometries, and only a similar dihedral aperture between the two end benzene rings (in both triarylamine groups) is appreciated. In what follows, we will see how these different structural patterns induce slightly different spectroscopic properties between the studied sensitizers.

The most interesting excited electronic state of the D*n* dyes as molecular sensitizers is the lowest excited singlet. The ground to first excited state transition has a $\pi \rightarrow \pi^*$ nature with an important charge transfer character. Thus, although other allowed low-lying electronic transitions are present in the D*n* family,[7] we focus our efforts on the understanding of the mentioned lowest excited state.

The One Electron Picture. Before analyzing the set of results obtained with the several methodologies announced in the Computational Details section, we believe it is worth it to set a general frame that will help to understand the results. To that purpose and to qualitatively explain the role of different chemical substitutions, we analyze the properties of the molecular orbitals of the D*n* family. We are especially interested in understanding the different energy gaps between the frontier orbitals, which should give us some hints about the subtle differences in their spectroscopic behavior. In order to avoid redundancies, we restrict this discussion to the results obtained with the ωB97X functional and the 6-31G(d) atomic basis set. Similar qualitative conclusions could be reached if we would pick the molecular orbitals obtained with another approach. We will also compare orbitals obtained from gas phase and ethanol solution within the SM8 model calculations.

Although the π-like HOMO of D5 is mainly localized at the triarylamine group, it noticeably expands toward the thiophene, probably due to the coplanarity of the fragments (Figure 2). On the other hand, the LUMO is basically localized at the thiopene and cyano-acrylate fragments, and only some small π^* contribution on the closer benzene ring is obtained.

The p-electrons from the two methoxy oxygen atoms in D9 extend the π-system conjugation in the HOMO and HOMO−1, adding some extra antibonding interaction, which slightly destabilizes the two highest occupied orbitals. Meanwhile, the LUMO is basically unaffected by the methoxy substitution, resulting in an appreciable decrease of the energy gaps with respect to D5 (Figure 2).

The main part of the electronic density in the D7 (and D11) HOMO orbital is disposed along the triarylamine group, which is collinear to the thiophene and cyano-acrylate groups, and like in the D5 (D9) case, it delocalizes over the thiophene. On the other hand, the second triarylamine, almost perpendicular to the main molecular direction, has a less important contribution to the orbital. In addition, the small loss of planarity in D7 (D11) explained above seems to only very mildly affect the energies of the occupied orbitals, slightly pushing them to higher values. The strong localization of the LUMO orbital in D7 (and D11) avoids any major difference with respect to the D5 (D9) LUMO caused by the nonplanarity effect. This would explain the energy similarities between D5 and D7 (D9 and D11). Finally, the methoxy substitution in D7 to D11 conduces to a reduction of the HOMOs to LUMO energy separation, very similarly to the D5/D9 case. The present HOMOs and LUMOs resemble those of the similar DS-3, DS-4, and DS-5 dyes explored in a recent study.[57]

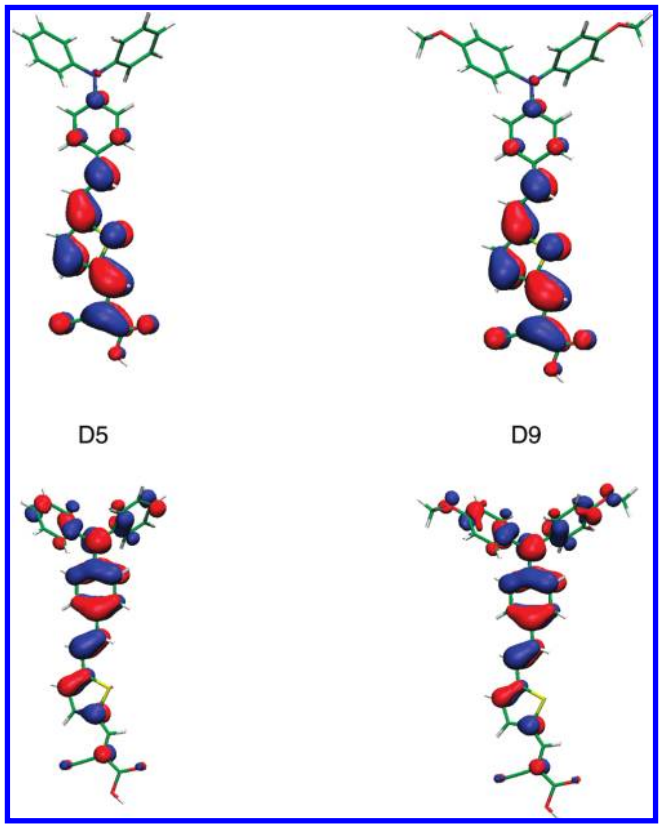

Figure 2. Isodensity surface plots of HOMO (down) and LUMO (up) orbitals at the ωB97X/6-31G(d) computational level in the gas phase for the D5 (left) and D9 (right) molecular dyes. A 0.03 cutoff has been used in all cases.

When the molecular orbitals are computed within the SM8 model (ethanol as the solvent), very similar results are obtained. The most significant difference in the presence of the solvent is a ~0.1 eV stabilization of the LUMO due to the localized character of the orbital, which arises from hydrogen bonding and the polarity of the ethanol solvent (ε = 24.85).

S_0 to S_1 Vertical Transition Energies. Computed vertical energy gaps in the gas phase and ethanol are shown and compared to experimental absorption maxima in ethanol solution[7] in Table 1.

The solvent−solute interaction has been included at the structural level through geometry optimization of D*n* dyes within the SM8 model, and also at the electronic structure level, incorporating the environment effects in the computation of the ground and excited states. The computation of D*n* dyes in ethanol results in a moderate shift to lower absorption frequencies with respect to the gas phase calculations for all methods. This shift is almost constant for the CIS, ωB97, and ωB97X energies, about 0.05, 0.08, and 0.07 eV on average, respectively. The solvent effect in B3LYP is less constant but of similar magnitude (~0.10 eV). On the other hand, maybe due to the fact that the wave function has not been relaxed in the excited state in the presence of the solvent, the solvation redshift is considerably larger, about 0.15−0.21 eV, when CIS is corrected to the second-order perturbation theory in the CIS(D) and SOS-CIS(D) methods.

Although the small redshift (about 0.1 eV) of the absorption band due to methoxy substitution between D5/D9 and D7/D11 is well recovered by B3LYP, as a result of the charge transfer nature of these $\pi\rightarrow\pi^*$ transitions, vertical energy gaps to the first singlet are dramatically underestimated.[58–60] The loss of planarity in the larger D7 and D11 dyes decreases the delocalization of the orbitals, especially the HOMO, increasing the charge transfer character of the transition. This is reflected as a more severe underestimation of the transition by B3LYP (>0.7 eV) in the computation of D7 and D11 dyes. On the other hand, the LC functionals improve this ill behavior of standard functionals, and the computed energies are closer to experimental results. In this case, ωB97 and ωB97X overcorrect the long-range charge transfer transition failure of the standard functionals. The ωB97 functional systematically overestimates the lowest $\pi\rightarrow\pi^*$ transitions in D*n* dyes by approximately 0.20 eV, while this effect is less pronounced with the inclusion of a small fraction of short-range Hartree−Fock exchange in ωB97X (the overestimation is reduced to 0.15 eV on average). As with B3LYP, both LC functionals are also able to correctly obtain the 0.1 eV redshift by methoxy substitution in D9 and D11.

CIS satisfactorily reproduces the 0.1 eV redshift by methoxy substitution, but as a result of the lack of dynamical correlation, all CIS transition energies present a systematic overestimation with a mean absolute error (MAE) of 0.40 eV with respect to experimental absorption maxima, which is a common feature of the CIS method in the computation of valence excitations of organic molecules. The inclusion of dynamical correlation through second-order perturbation theory noticeably corrects the overestimation in CIS, decreasing the transition energies in CIS(D) and SOS-CIS(D) by 0.48 and 0.67 eV on average, respectively. This correction drives to CIS(D) energies which are very close to experimental absorption maxima (MAE = 0.08 eV) but is a bit large in SOS-CIS(D). These results seem to indicate that, although it was previously shown[39] that only considering the scaled opposite spin component of the second order

Table 1. Transition Energies (in eV) of the D*n* Dyes in the Gas Phase and Ethanol Solution (SM8 solvation model) for All Studied Excited State Methods, Computed for the B3LYP/6-31G(d) SM8 Optimized Geometries with the 6-31+G(d) Basis Set

method	D5	D7	D9	D11
		Vacuum		
B3LYP	2.28	2.06	2.18	1.96
ωB97	3.10	3.09	3.03	2.96
ωB97X	3.04	3.01	2.96	2.88
CIS	3.24	3.23	3.19	3.13
SOS-CIS(D)	2.75	2.72	2.64	2.53
CIS(D)	2.92	2.89	2.82	2.72
		Ethanol, SM8		
B3LYP	2.16	2.07	1.98	1.88
ωB97	3.04	3.01	2.95	2.88
ωB97X	2.97	2.94	2.87	2.81
CIS	3.20	3.18	3.13	3.07
SOS-CIS(D)	2.59	2.56	2.43	2.35
SOS-CIS(D)[a]	2.72	2.68	2.59	2.48
CIS(D)	2.77	2.75	2.62	2.54
CIS(D)[a]	2.89	2.84	2.77	2.66
experimental	**2.81**	**2.81**	**2.68**	**2.71**

[a] The solvent effects in CIS second-order corrected methods were obtained from the gas phase vs SM8 differences obtained in CIS.

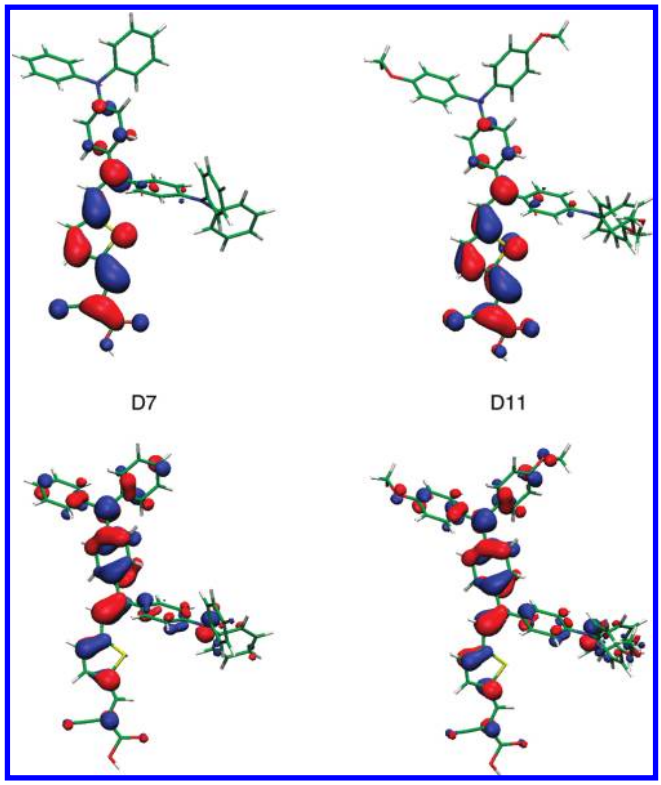

Figure 3. Isodensity surface plots of HOMO (down) and LUMO (up) orbitals at the ωB97X/6-31G(d) computational level in the gas phase for the D7 (left) and D11 (right) molecular dyes. A 0.03 cutoff has been used in all cases

correction of CIS slightly increases the perturbation correction and improves the accuracy of the computed valence $\pi\rightarrow\pi^*$ transitions in the gas phase with respect to CIS(D), the large solvatochromic redshifts (~0.2 eV) in the perturbationally corrected methods compensate for the slight to high excitation energies in CIS(D) but result in a systematic underestimation in SOS-CIS(D) (MAE = 0.27 eV). When the solvation correction coming from CIS is added to the SOS-CIS(D) in gas phase (Table 1), excitation energies are obtained in substantially better agreement with the experimental values, with a MAE = 0.14 eV underestimation. The same treatment of the solvation effects slightly improves CIS(D) energies (MAE = 0.06) in CIS(D). Both second-order corrected methods keep, in general, the same transition energy shift to lower frequencies between D5/D9 and D7/D11 obtained by CIS.

S_0 to S_1 Transition Amplitudes. The transition amplitudes obtained from the TDDFT and CIS methods give a quantitative description of the orbital contributions in the excited state wave function. In the D*n* family, the energetically lowest absorptions stem from $\pi\rightarrow\pi^*$ transitions and can be mainly described as HOMO to LUMO electronic promotions (see isodensity surface plots in Figures 2 and 3). For all explored methods but B3LYP, this amplitude, in the gas phase, constitutes about 60−70% of the final state, whereas HOMO−1 to LUMO in D5 and D9 and HOMO−2 to LUMO in D7 and D11 are responsible for 20−25%. Other possible contributions like HOMO to LUMO+1 are much less important. These compositions do not suffer any significant modification when obtained in ethanol, either using the Onsager, SS(V)PE, or SM8 solvation models analyzed below.

Table 2. Basis Set Dependence of the Transition Energies (in eV) of the D*n* Dyes in Gas Phase for All Studied Excited State Methods[a]

method	6-31G	6-31G(d)	6-31+G	6-31+G(d)
		D5		
ωB97	3.24	3.18	3.16	3.10
ωB97X	3.16	3.11	3.08	3.04
CIS	3.35	3.32	3.28	3.24
SOS-CIS(D)	3.05	2.85	2.95	2.75
CIS(D)	3.13	3.02	3.02	2.92
		D7		
ωB97	3.21	3.16	3.14	3.09
ωB97X	3.13	3.08	3.06	3.01
CIS	3.33	3.29	3.28	3.23
SOS-CIS(D)	3.02	2.81	2.92	2.72
CIS(D)	3.09	2.98	3.00	2.89
		D9		
ωB97	3.16	3.11	3.09	3.03
ωB97X	3.08	3.04	3.01	2.96
CIS	3.31	3.27	3.23	3.19
SOS-CIS(D)	2.94	2.74	2.84	2.64
CIS(D)	3.03	2.92	2.92	2.82
		D11		
ωB97	3.07	3.02	3.01	2.96
ωB97X	2.99	2.95	2.93	2.88
CIS	3.23	3.19	3.17	3.13
SOS-CIS(D)	2.82	2.62	2.72	2.53
CIS(D)	2.91	2.81	2.81	2.72

[a] All energies were computed on the B3LYP/6-31G(d) optimized geometries in ethanol (SM8).

On the other hand, the HOMO to LUMO contribution in B3LYP accounts for ~95% of the transition of D5 and D9 dyes, whereas in D7 and D11, the electronic transit is built up from similar weights of the HOMO−1 and HOMO to LUMO excitations. When the ethanol effects are introduced, D5 and D9 transition amplitudes remain very similar to the gas phase, while becoming ~70% and ~30% for HOMO−1 and HOMO to LUMO for D7 and D11 molecules. This different behavior in B3LYP is symptomatic of the failures already present in the important underestimation of excitation energies.

Transition Energy Dependence on the Basis Set. The election of a basis set in the computation of molecular electronically excited states becomes crucial if one intends to obtain accurate results.[61–63] In this section, we explore how excitation energies to the lowest singlet in D*n* dyes vary with the employed basis. We do not pretend to produce a benchmark study, but we rather want to provide some hints of the importance of the basis set in computing the S_0 to S_1 transitions. Because of the failure of B3LYP to quantitatively capture the lowest singlet excited state of D*n* dyes, we have not included it in this study. The interested reader in the B3LYP excitation energies dependence on the basis set is referred to the Supporting Information (Tables S1 and S2).

As a result of the lack of polarization and diffusion functions, the excitations computed with the 6-31G basis (Table 2) are substantially higher compared to those with the larger 6-31+G(d) basis. This difference is on the order of 0.1 eV for CIS and TDDFT and even larger for CIS(D) and SOS-CIS(D), about 0.2 and 0.3 eV, respectively. When

Table 3. Molecular Geometry Dependence of the Transition Energies (in eV) of the D*n* Dyes in Ethanol Solution (SM8 model) for All Studied Excited State Methods[a]

	optimized geometry			
method	B3LYP	ωB97	ωB97X	SOSMP2
	D5 (ΔE_{expt} = 2.81 eV)			
ωB97	3.04	3.39	3.35	3.36
ωB97X	2.97	3.29	3.26	3.27
CIS	3.20	3.57	3.53	3.53
SOS-CIS(D)	2.59	3.09	3.03	3.03
SOS-CIS(D)[b]	2.72	3.15	3.11	3.10
CIS(D)	2.77	3.19	3.15	3.15
CIS(D)[b]	2.89	3.25	3.21	3.21
	D7 (ΔE_{expt} = 2.81 eV)			
ωB97	3.01	3.39	3.35	3.32
ωB97X	2.94	3.31	3.28	3.24
CIS	3.18	3.60	3.56	3.52
SOS-CIS(D)	2.56	3.06	3.02	2.98
SOS-CIS(D)[b]	2.68	3.16	3.11	3.05
CIS(D)	2.75	3.18	3.15	3.11
CIS(D)[b]	2.84	3.25	3.22	3.17
	D9 (ΔE_{expt} = 2.68 eV)			
ωB97	2.95	3.32	3.27	3.27
ωB97X	2.87	3.22	3.18	3.18
CIS	3.13	3.53	3.48	3.47
SOS-CIS(D)	2.43	2.99	2.93	2.91
SOS-CIS(D)[b]	2.59	3.07	3.01	3.00
CIS(D)	2.62	3.09	3.04	3.03
CIS(D)[b]	2.77	3.16	3.12	3.10
	D11 (ΔE_{expt} = 2.71 eV)			
ωB97	2.88	3.28	3.24	3.26
ωB97X	2.81	3.19	3.15	3.18
CIS	3.07	3.49	3.46	3.47
SOS-CIS(D)	2.35	2.90	2.85	2.88
SOS-CIS(D)[b]	2.48	2.98	2.94	2.94
CIS(D)	2.54	3.01	2.97	3.01
CIS(D)[b]	2.66	3.08	3.04	3.06

[a] All energies were computed with the 6-31+G(d) basis on the (B3LYP, ωB97, ωB97X, SOSMP2)/6-31G(d) optimized geometries in ethanol (SM8). [b] The solvent effects in CIS second-order corrected methods were obtained from the gas phase vs SM8 differences obtained in CIS.

polarization functions are included, the excitation energies are systematically shrunk. This lowering is about 0.05 eV for all transitions computed by CIS and TDDFT, whereas this effect is twice as large in CIS(D) and four times larger (0.20 eV) in SOS-CIS(D). The reduction of transition energies by diffuse functions, i.e., the 6-31+G column in Table 2, has a similar magnitude to the one obtained in 6-31G(d), except in SOS-CIS(D), where, as in CIS(D), the effect accounts for a ~0.1 eV decrease in the excitation energies. These comparisons from Table 2 indicate that both polarization and diffuse functions substantially contribute to the final states, diminishing the S_0 to S_1 gaps by 0.10 to 0.30 eV.

Very similar results are obtained when excitation energies are computed for the different basis sets and in the presence of ethanol as a solvent (see Table S2 of Supporting Information).

Transition Energy Dependence on the Geometry Optimization. The molecular geometry used in electronic structure calculations can be a key factor when computing energies for ground and excited states. In Table 3, we compare the D*n* vertical transition energies in ethanol obtained from four different geometry optimization levels, i.e., B3LYP, ωB97, ωB97X, and SOSMP2.

The best performance of computed vertical energies is obtained when B3LYP is employed in the optimization of the ground state. Meanwhile, ωB97, ωB97X, and SOSMP2 geometries produce too large excitation energies in all cases. Compared to B3LYP-geometry results, transitions from ωB97X geometries are 0.30 to 0.50 eV higher. This difference is slightly increased (~0.05 eV) when ωB97 geometries are employed. Excitations from SOSMP2 optimized geometries are very similar to the ones obtained from ωB97X. These results have to be (only) seen as a consequence of a more favorable error compensation in B3LYP/6-31G(d) optimized geometries in the computation of D*n* S_0 to S_1 transitions.

Gas phase and ethanol solution (including B3LYP transitions) energy comparisons are presented as Supporting Information (Tables S3 and S4).

Transition Energy Dependence on the Solvation Model. Here, we perform a systematic analysis over three possible approaches to account for the solute−solvent interaction, i.e., the Onsager reaction field model[52] up to the 15th multipole order expansion, Surface and Simulation of Volume Polarization for Electrostatics (SS(V)PE),[53–55] and the SM8 solvation model,[45] in the computation of the D*n* dyes' excitation energies in ethanol solution. The larger energy stabilization of the LUMOs when the D*n* electronic structure is computed in solution makes us expect smaller energy gaps when the ethanol presence is modeled. The comparison of D*n* transition energies computed in the gas phase and with the three different solvation models is shown in Table 4.

In the Onsager model, specific electrostatic solute−solvent interactions are not treated, and the solute is enclosed in a spherical cavity. Most likely due to the neglect of specific electrostatic interactions, the excitation energies are very close to the gas phase results. In general, there is a small redshift (≤0.07 eV) with respect to gas phase energies for D5, D7, and D11. On the other hand, the D9 transition energies suffer similar magnitude frequency displacement but to larger energies. This behavior is common to all wave function-based and TDDFT explored methods. The SS(V)PE model treats electrostatic solute−solvent interactions by solving Poisson's equation at the cavity surface defined as the isodensity surface or a spherical cavity (dispersion and cavitation are neglected). Since the computations could not be converged for isodensity surfaces, solvation had to be computed using a spherical cavity. In this case, the electrostatic interactions are not localized properly. Surprisingly, SS(V)PE transition energies for the smaller dyes (D5 and D9) are slightly higher, between 0.03 and 0.28 eV, than the gas phase computed energies. Meanwhile, there is a small decrease in the D7 and D11 molecules, although the difference from the gas phase values is no larger than 0.07 eV. Since hydrogen bonding (with the ethanol solvent) is mainly electrostatic, the neglect of electrostatic interactions (Onsager) or its approximate treatment (SS(V)PE with a spherical cavity) is responsible for the errors. In contrast,

Table 4. Transition Energies (in eV) of the D*n* Dyes in Ethanol Solution for All Studied Excited State Methods[a]

method	vacuum	Onsager	SS(V)PE	SM8
	D5 (ΔE_{expt} = 2.81 eV)			
B3LYP	2.34	2.31	2.42	2.20
ωB97	3.18	3.19	3.25	3.12
ωB97X	3.11	3.12	3.18	3.04
CIS	3.32	3.31	3.35	3.25
SOS-CIS(D)	2.85	2.84	2.96	2.59
SOS-CIS(D)[b]		2.84	2.88	2.78
CIS(D)	3.02	3.01	3.13	2.79
CIS(D)[b]		3.02	3.05	2.96
	D7 (ΔE_{expt} = 2.81 eV)			
B3LYP	2.11	2.05	2.06	1.97
ωB97	3.16	3.13	3.13	3.09
ωB97X	3.08	3.05	3.05	3.01
CIS	3.29	3.27	3.27	3.23
SOS-CIS(D)	2.81	2.74	3.02	2.57
SOS-CIS(D)[b]		2.79	2.79	2.75
CIS(D)	2.98	2.91	2.91	2.76
CIS(D)[b]		2.96	2.96	2.92
	D9 (ΔE_{expt} = 2.68 eV)			
B3LYP	2.23	2.27	2.46	2.08
ωB97	3.11	3.16	3.26	3.05
ωB97X	3.04	3.09	3.19	2.97
CIS	3.27	3.29	3.35	3.20
SOS-CIS(D)	2.74	2.81	3.02	2.48
SOS-CIS(D)[b]		2.76	2.82	2.67
CIS(D)	2.92	2.99	3.18	2.69
CIS(D)[b]		2.94	3.00	2.86
	D11 (ΔE_{expt} = 2.71 eV)			
B3LYP	2.01	1.96	1.97	1.83
ωB97	3.02	2.99	2.99	2.95
ωB97X	2.95	2.92	2.91	2.87
CIS	3.19	3.17	3.16	3.12
SOS-CIS(D)	2.62	2.56	2.55	2.38
SOS-CIS(D)[b]		2.60	2.64	2.56
CIS(D)	2.81	2.75	2.74	2.58
CIS(D)[b]		2.79	2.78	2.74

[a] Solvation model dependence computed for the B3LYP/6-31G(d) SM8 optimized geometries with the 6-31G(d) basis set. [b] The solvent effects in CIS second order corrected methods were obtained from the gas phase vs SS(V)PE and SM8 differences obtained in CIS, respectively.

electrostatic interactions are treated with SM8, which is based on the generalized Born method for electrostatics augmented with atomic surface tensions for first-solvation-shell effects, and the deviation of the electrostatics from what can be calculated using only the bulk dielectric constant. Furthermore, cavitation and dispersion are included. Thus, all SM8 computed transition energies show a moderate redshift with respect to gas phase values. This behavior is almost constant (between 0.06 and 0.08 eV) for all transitions computed by TDDFT with the ωB97 and ωB97X functionals and the CIS method, and a little bit larger in B3LYP ($\sim$0.15 eV). As has been discussed above, the solvation redshift is considerably larger, about 0.25 eV, when CIS is corrected to the second order in the CIS(D) and SOS-CIS(D) methods. When the solvation correction coming from CIS is added to the SOS-CIS(D) in the gas phase, excitation energies are obtained in much better agreement with the experimental values.

The more accurate results obtained with SM8 are due to the approximate treatment of hydrogen bonding with the solvent. The present organic dyes are far from being spherically shaped, but the Onsager and SS(V)PE solvation models employed here require the dyes to be surrounded by a spherical cavity. As shown, computations with shape-adapted cavities, as it is done in SM8, seem much more convenient in these cases.

Conclusions

The ground and first excited singlet states of the D5, D7, D9, and D11 molecular dyes have been studied. Computed excitation energies between them within TDDFT and wave-function-based methods have been compared to experimental absorption maxima, and the roles of different geometrical features and chemical substitutions have been discussed.

The smaller D5 and D9 dyes have a rather linear geometry and present localized HOMOs and LUMOs, especially the latter, at the two different molecular ends. The electron−hole separation in the electronic transition to the excited singlet results in a charge transfer nature of the excitation. The substitution of a second triarylamine group in D7 and D11 does not change the general picture of the electronic transition. The methoxy substitution in D9 and D11 produces a decrease of the excitation due to an extra antibonding interaction in the HOMO caused by the p-orbital of oxygen atoms with the benzene ring.

As far as the agreement with experimental results of transition energies to the first excited singlet is concerned, the CIS(D) method is superior to the LC ωB97 and ωB97X functionals. The scaled opposite spin version of CIS(D) represents an attractive alternative to CIS(D), especially due to its lower computational cost, although one must be careful when the solute−solvent interactions are included. Within the TDDFT realm, the ωB97X approach is the most promising tested functional in the computation of this kind of molecular dyes. On the other hand, B3LYP should not be the chosen method for routine screening of excitation energies of such molecules. The charge transfer nature of the first excited singlet produces catastrophic results when standard functionals, such as B3LYP, are used, which could drive us to wrong conclusions. Moreover, the magnitude of this underestimation, as has been shown between D5/D9 and D7/D11, strongly depends on the molecular characteristics, making this functional inappropriate for general comparisons.

The variation in the computed energy gaps due to different basis sets has been studied for all wave function-based and TDDFT employed methods. Similar contributions were found from polarization and diffuse functions when comparing 6-31G, 6-31+G, 6-31G(d), and 6-31+G(d) results. Transition energy dependence on the molecular geometry has been explored using four different optimization approaches. The best results were obtained when ground state geometries were optimized by the B3LYP functional. The use of ωB97, ωB97X, or SOSMP2 geometries drives to overestimation of the energy gaps. Finally, the role of ethanol as a solvent has been taken into account in the computation of optimized geometries and electronic structure calculations for three different solvation models. SM8 reproduces the expected solvent-induced redshift in the vertical excitation energies correctly. The deficiencies in the two other explored solvation models, i.e., Onsager and SS(V)PE, are due to the neglect

or too approximate treatment of specific electrostatic solute−solvent interactions.

Acknowledgment. Financial support for this work was provided by the Spanish Ministerio de Ciencia e Innovación through project CTQ2008-06670-C02-02/BQU, the Generalitat de Catalunya through project 2009SGR-1459, and the Office of Basic Energy Sciences of the U.S. Department of Energy through the LBL Ultrafast Center, with additional support from the Director, Office of Energy Research, Office of Basic Energy Sciences, Chemical Sciences Division of the U.S. Department of Energy under Contract DE-AC0376SF00098, and supercomputer time from NERSC. D.C. gratefully acknowledges the Ramón y Cajal program for financial support and Professor Martin Head-Gordon for his comments, suggestions, and fruitful discussions on several of the topics presented in this work.

Supporting Information Available: Tables giving basis set and molecular geometry dependences. This material is available free of charge via the Internet at http://pubs.acs.org.

References

(1) Nazeeruddin, M. K.; De Angelis, F.; Fantacci, S.; Selloni, A.; Viscardi, G.; Liska, P.; Ito, S.; Takeru, B.; Grätzel, M. *J. Am. Chem. Soc.* **2005**, *127*, 16835.

(2) Grätzel, M. *J. Photochem. Photobiol., A* **2004**, *164*, 3.

(3) Hara, K.; Sato, T.; Katoh, R.; Furube, A.; Ohga, Y.; Shinpo, A.; Suga, S.; Sayama, K.; Sugihara, H.; Arakawa, H. *J. Phys. Chem. B* **2003**, *107*, 597.

(4) Horiuchi, T.; Miura, H.; Sumioka, K.; Uchida, S. *J. Am. Chem. Soc.* **2004**, *126*, 12218.

(5) Kim, S.; Lee, J. K.; Kang, S. O.; Ko, J.; Yum, J. H.; Fantacci, S.; De Angelis, F.; Di Censo, D.; Nazeeruddin, M. K.; Grätzel, M. *J. Am. Chem. Soc.* **2006**, *128*, 16701.

(6) Hagberg, D. P.; Edvinsson, T.; Marinado, T.; Boschloo, G.; Hagfeldt, A.; Sun, L. *Chem. Commun.* **2006**, 2245.

(7) Hagberg, D. P.; Yum, J.-H.; Lee, H.; De Angelis, F.; Marinado, T.; Karlsson, K. M.; Humphry-Baker, R.; Sun, L.; Hagfeldt, A.; Grätzel, M.; Nazeeruddin, M. K. *J. Am. Chem. Soc.* **2008**, *130*, 6259.

(8) Rowe, D. J. *Rev. Mod. Phys.* **1968**, *40*, 153.

(9) Stanton, J. F.; Bartlett, R. J. *J. Chem. Phys.* **1993**, *98*, 7029.

(10) Emrich, K. *Nucl. Phys. A* **1981**, *351*, 379.

(11) Geertsen, J.; Rittby, M.; Bartlett, R. J. *Chem. Phys. Lett.* **1989**, *164*, 57.

(12) Levchenko, S. V.; Krylov, A. I. *J. Chem. Phys.* **2004**, *120*, 175.

(13) Monkhorst, H. J. *Int. J. Quantum Chem., Symp.* **1977**, *11*, 421.

(14) Sekino, H.; Bartlett, R. J. *Int. J. Quantum Chem.* **1984**, *26*, 255.

(15) Janet, E. D. B.; Ditchfield, R.; Pople, J. A. *J. Chem. Phys.* **1971**, *55*, 2236.

(16) Nakatsuji, H.; Hirao, K. *J. Chem. Phys.* **1978**, *68*, 2053.

(17) Nakatsuji, H. *Chem. Phys. Lett.* **1991**, *177*, 331.

(18) Siegbahn, P. E. M. In *Methods in Computational Molecular Physics*; Diercksen, G. H. F., Ed.; Reidel: Dordrecht, The Netherlands, 1983; p 189.

(19) *Recent Advances in Multi-reference Methods*; World Scientific: Singapore, 1999.

(20) Mukherjee, D.; Pal, S.; Per-Olov, L. In *Advanced Quantum Chemistry*;Academic Press: New York, 1989; Vol 20, p 291.

(21) Roos, B. O.; Andersson, K.; Fülscher, M. P. *Chem. Phys. Lett.* **1992**, *192*, 5.

(22) Nakano, H. *J. Chem. Phys.* **1993**, *99*, 7983.

(23) Nakano, H. *Chem. Phys. Lett.* **1993**, *207*, 372.

(24) Malmqvist, P. Å.; Pierloot, K.; Shahi, A. R. M.; Cramer, C. J.; Gagliardi, L. *J. Chem. Phys.* **2008**, *128*, 204109.

(25) Nakano, H.; Uchiyama, R.; Hirao, K. *J. Comput. Chem.* **2002**, *23*, 1166.

(26) Ebisuzaki, R.; Watanabe, Y.; Nakano, H. *Chem. Phys. Lett.* **2007**, *442*, 164.

(27) Miyajima, M.; Watanabe, Y.; Nakano, H. *J. Chem. Phys.* **2006**, *124*, 044101.

(28) Gross, E. K. U.; Kohn, W. *Phys. Rev. Lett.* **1985**, *55*, 2850.

(29) Runge, E.; Gross, E. K. U. *Phys. Rev. Lett.* **1984**, *52*, 997.

(30) Cohen, A. J.; Mori-Sanchez, P.; Yang, W. *Science* **2008**, *321*, 792.

(31) Perdew, J. P.; Zunger, A. *Phys. Rev. B* **1981**, *23*, 5048.

(32) Zhao, Y.; Truhlar, D. G. *Acc. Chem. Res.* **2008**, *41*, 157.

(33) Sobolewski, A. L.; Domcke, W. *Chem. Phys.* **2003**, *294*, 73.

(34) Dreuw, A.; Weisman, J. L. *J. Chem. Phys.* **2003**, *119*, 2943.

(35) Dreuw, A.; Head-Gordon, M. *J. Am. Chem. Soc.* **2004**, *126*, 4007.

(36) Dreuw, A.; Fleming, G. R.; Head-Gordon, M. *Phys. Chem. Chem. Phys.* **2003**, *5*, 3247.

(37) Head-Gordon, M.; Rico, R. J.; Oumi, M.; Lee, T. J. *Chem. Phys. Lett.* **1994**, *219*, 21.

(38) Head-Gordon, M.; Grana, A. M.; Maurice, D.; White, C. A. *J. Phys. Chem.* **1995**, *99*, 14261.

(39) Rhee, Y. M.; Head-Gordon, M. *J. Phys. Chem. A* **2007**, *111*, 5314.

(40) Becke, A. D. *J. Chem. Phys.* **1993**, *98*, 5648.

(41) Lee, C.; Yang, W.; Parr, R. G. *Phys. Rev. B* **1988**, *37*, 785.

(42) Chai, J.-D.; Head-Gordon, M. *J. Chem. Phys.* **2008**, *128*, 084106.

(43) Jung, Y.; Lochan, R. C.; Dutoi, A. D.; Head-Gordon, M. *J. Chem. Phys.* **2004**, *121*, 9793.

(44) Lochan, R. C.; Shao, Y.; Head-Gordon, M. *J. Chem. Theory Comput.* **2007**, *3*, 988.

(45) Marenich, A. V.; Olson, R. M.; Kelly, C. P.; Cramer, C. J.; Truhlar, D. G. *J. Chem. Theory Comput.* **2007**, *3*, 2011.

(46) Hehre, W. J.; Ditchfield, R.; Pople, J. A. *J. Chem. Phys.* **1972**, *56*, 2257.

(47) Hariharan, P. C.; Pople, J. A. *Theor. Chem. Acc.* **1973**, *28*, 213.

(48) Christof, H.; Florian, W. *J. Chem. Phys.* **2000**, *113*, 5154.

(49) Hattig, C.; Hald, K. *Phys. Chem. Chem. Phys.* **2002**, *4*, 2111.

(50) Wilson, A. K.; Almlöf, J. *Theor. Chem. Acc.* **1997**, *95*, 49.

(51) Hirata, S.; Head-Gordon, M. *Chem. Phys. Lett.* **1999**, *314*, 291.

(52) Onsager, L. *J. Am. Chem. Soc.* **1936**, *58*, 1486.

(53) Chipman, D. M. *J. Chem. Phys.* **2000**, *112*, 5558.

(54) Chipman, D. M. *Theor. Chem. Acc.* **2002**, *107*, 80.

(55) Chipman, D. M.; Dupuis, M. *Theor. Chem. Acc.* **2002**, *107*, 90.

(56) Shao, Y.; Molnar, L. F.; Jung, Y.; Kussmann, J.; Ochsenfeld, C.; Brown, S. T.; Gilbert, A. T. B.; Slipchenko, L. V.; Levchenko, S. V.; O'Neill, D. P.; DiStasio, R. A., Jr.; Lochan, R. C.; Wang, T.; Beran, G. J. O.; Besley, N. A.; Herbert, J. M.; Lin, C. Y.; Voorhis, T. V.; Chien, S. H.; Sodt, A.; Steele, R. P.; Rassolov, V. A.; Maslen, P. E.; Korambath, P. P.; Adamson, R. D.; Austin, B.; Baker, J.; Byrd, E. F. C.; Dachsel, H.; Doerksen, R. J.; Dreuw, A.; Dunietz, B. D.; Dutoi, A. D.; Furlani, T. R.; Gwaltney, S. R.; Heyden, A.; Hirata, S.; Hsu, C.-P.; Kedziora, G.; Khalliulin, R. Z.; Klunzinger, P.; Lee, A. M.; Lee, M. S.; Liang, W.; Lotan, I.; Nair, N.; Peters, B.; Proynov, E. I.; Pieniazek, P. A.; Rhee, Y. M.; Ritchie, J.; Rosta, E.; Sherrill, C. D.; Simmonett, A. C.; Subotnik, J. E.; Woodcock, H. L., III; Zhang, W.; Bell, A. T.; Chakraborty, A. K. *Phys. Chem. Chem. Phys.* **2006**, *8*, 3172.

(57) Li, G.; Jiang, K.-J.; Bao, P.; Li, Y.-F.; Li, S.-L.; Yang, L.-M. *New J. Chem.* **2009**, *33*, 868.

(58) Dreuw, A.; Weisman, J. L.; Head-Gordon, M. *J. Chem. Phys.* **2003**, *119*, 2943.

(59) Dreuw, A.; Head-Gordon, M. *Chem. Rev.* **2005**, *105*, 4009.

(60) Sobolewski, A. L.; Domcke, W. *Chem. Phys.* **2003**, *294*, 73.

(61) Schreiber, M.; Silva-Junio, M. R.; Sauer, S. P. A.; Thiel, W. *J. Chem. Phys.* **2008**, *128*, 134110.

(62) Silva-Junio, M. R.; Schreiber, M.; Sauer, S. P. A.; Thiel, W. *J. Chem. Phys.* **2008**, *129*, 104103.

(63) Jacquemin, D.; Wathelet, V.; Perpète, E. A.; Adamo, C. *J. Chem. Theory Comput.* **2009**, *5*, 2420.

CT100069Q